ELSEVIER

Journal of Alloys and Compounds 444–445 (2007) 438–442

Journal of ALLOYS AND COMPOUNDS

www.elsevier.com/locate/jallcom

Inductive cold crucible melting of actinide-bearing murataite-based ceramics

S.V. Stefanovsky [a,*], A.G. Ptashkin [a], O.A. Knyazev [a], S.A. Dmitriev [a], S.V. Yudintsev [b], B.S. Nikonov [b]

[a] *SIA Radon, 7th Rostovskii Lane 2/14, Moscow 119121, Russia*
[b] *Institute of Geology of Ore Deposits RAS, Staromonetny Lane 35, Moscow 119117, Russia*

Received 3 July 2006; received in revised form 10 January 2007; accepted 11 January 2007
Available online 18 January 2007

Abstract

Murataite-based ceramics doped with U or Th were produced by inductive cold crucible melting (ICCM) at operating frequencies of 1.76 and 5.28 MHz and examined using X-ray diffraction and scanning and transmission electron microscopy. Three distinct murataite polytypes were identified in the U-bearing ceramics: a five- (5C), eight- (8C), and three-fold (3C) fluorite unit cell crystals that respectively make up what is designated as the core, intermediate and rim zones. In contrast, the Th-bearing ceramic contained only the five-fold (5C) fluorite unit cell polytype. The core zone of the murataite in the U-bearing specimens is characterized by UO_2 concentrations as high as 12.1 wt%, which successively diminishes in concentration through the intermediate zone to the rim, the latter of which contains 5.2 wt% UO_2. On the other hand, Th distribution within the murataite crystals is uniform. The difference in phase composition and actinide partitioning in the ceramics is influenced by synthesis conditions. Larger cold crucible size ensures lower crystallization rate yielding zoned crystals with maximum actinide concentration in the core of the murataite crystals that minimizes exposure of the actinide elements to potential leach solutions.

Keywords: Ceramics; Crystal growth; Microstructure; Scanning electron microscopy; SEM; X-ray diffraction

1. Introduction

An inductive cold crucible melting (ICCM) is an effective method for growing single crystals for various technical and jewelry purposes and for production of glassy and ceramic materials [1]. The ICCM is currently developed as an alternative to vitrification of high- (HLW) [2,3] and intermediate-level wastes (ILW) [4] in Joule-heated ceramic melters. The ICCM seems to be very promising method of HLW ceramization due to small dimensions of the equipment, a high-active hydrodynamic regime, and high temperature availability. This method was used to producing numerous ceramic waste forms (see, for example [5–8]). In one of the ICCM ceramics developed for immobilization of rare earth/actinide-bearing waste of the Russian spent fuel reprocessing plant "RT-1", we found a phase that accumulated more than 40% of the total uranium in the ceramic, which has been attributed to murataite [6]. This phase was earlier found in the ceramic designed for immobilization of Savannah River Plant defense waste [9]. Its natural analogue is a rare naturally-occurring mineral, murataite, whose structure has been investigated in details in [10].

The crystal structure of natural murataite with the idealized formula $A_6B_{12}C_4TX_{40-x}$ (A = Y, Na; B = Ti; C = Fe; T = Zn; X = O, F) according to [10] is cubic with space group $F\ \bar{4}3m$, $a = 14.89$ Å, $Z = 4$. The structure contains four distinct cationic sites: the A [8] – sites are eight-coordinated distorted cubes filled with large-sized cations ($REE^{3+/4+}$, $An^{3+/4+}$, Zr^{4+}, Ca^{2+}, Mn^{2+}); the B [6] – sites are octahedrally coordinated and filled with Ti^{4+}, Fe^{3+}, Al^{3+}, Nb^{5+} cations; the C [5] – sites are five-coordinated triangular bipyramids filled with Mn^{3+} and Fe^{3+} cations; and the T [4] – sites are tetrahedral filled with small cations (Zn^{2+}, Si^{4+}) in the naturally-occurred specimens and empty in the synthetic analogues. Recently we have shown [11] that the formula of the synthetic phase may be represented as $A_3B_6C_2O_{20-x}$ and its structure is considered as fluorite-derived with a three-fold elementary fluorite unit cell. Thus, the murataite structure is

* Corresponding author. Tel.: +7 495 919 3194.
E-mail address: profstef@mtu-net.ru (S.V. Stefanovsky).

0925-8388/$ – see front matter © 2007 Elsevier B.V. All rights reserved.
doi:10.1016/j.jallcom.2007.01.067

capable of accommodating a broad spectrum of elements with widely variable ionic radii including actinides, rare earths and iron group elements (potential corrosion products) that makes murataite an attractive candidate host phase for immobilization of actinide/rare earth-bearing wastes with complex chemical compositions [11,12].

It has also been established that pyrochlore $A^{VIII}{}_2B^{VI}{}_2O_7$ and murataite $A^{VIII}{}_3B^{VI}{}_6C^{V}{}_2O_{20-x}$, both having fluorite-derived structures with two- (2C) and three-fold (3C) fluorite unit cell, respectively [11–13], are end-members of the polysomatic series [11] comprising the phases with combined structures built from alternating pyrochlore (2C) and murataite (3C) modules (layers of atoms): 8C (3/2/3), 5C (3/2), and 7C (2/3/2). Based on a modular structure of the polytypes and combining formulae of the pyrochlore and murataite (3C polytype) their formulae were suggested to be $A_8B_{14}C_2O_{47-x}$, $A_5B_8C_2O_{27-x}$, and $A_7B_{10}C_2O_{34-x}$, respectively. The capability of the polytypes to accommodate actinides and rare earths (lanthanides) and zirconium increases in the row: 3C (murataite) < 8C < 5C < 7C < 2C (pyrochlore).

Because ceramics based on the pyrochlore/murataite series are capable of incorporating various waste elements, have high chemical durability [14] and radiation resistance comparable to pyrochlore [12,15], it is expedient to apply the ICCM to develop high-productive, compact, and remote operated process with high volume reduction yielding leach resistant waste form.

2. Experimental

Specified chemical compositions of the ceramics were as follows (wt%): 5 Al_2O_3, 10 CaO, 55 TiO_2, 10 MnO, 5 Fe_2O_3, 5 ZrO_2, 10 AnO_2 (An = U, Th). The UO_2-bearing ceramic (U-ICCM) was produced from an oxide mixture at the Radon bench-scale cold crucible (108 mm inner diameter, stainless steel) unit energized from a 1.76 MHz/60 kW generator (Fig. 1 left and upper right).

The ThO_2-bearing ceramic (Th-ICCM) was produced in a lab-scale unit with a 65 mm inner diameter copper cold crucible energized from a 5.28 MHz/10 kW generator (Fig. 1, lower right).

The samples were examined with X-ray diffraction using a Rigaku D/MAX-2200 diffractometer (Cu Kα radiation, voltage is 40 KeV, beam current is 30 mA, dwell time is 0.6 s, step size is 0.02°, 2-theta ranged between 5° and 75°, and Si as an internal standard), scanning electron microscopy with energy dispersive system (SEM/EDS) using a JSM-5300 + Link ISIS unit (voltage is 25 KeV, beam current is 1 nA, probe diameter is 1 to 3 μm, dwell time is 100 s; metals, oxides and fluorides were used as standards), and transmission electron microscopy (TEM) by selected area electron diffraction (SAED) pattern mode using a JEM-100c + KEVEX-5100 unit (resolution is 7 Å, accelerated voltage is 100 KeV).

3. Results

3.1. Preparation and characterization of the U-bearing ceramic

Production of the U-ICCM ceramic began with the inclusion of a SiC rod. The melting initiation process took 22 min and was followed by batch feeding in portions for 15 min, homogenization for 5 min, and the resulting melt, approximately 2.7 kg, was poured into a container to cool and crystallize. Because 2.7 kg of ceramic was produced for 20 min, the average productivity is 8.1 kg/h or a specific productivity of 900 kg/(m^2 h).

Both the ceramics were composed predominately of the target murataite-type phases and minor volumes of trace phases (Figs. 2 and 3). In the U-ICCM ceramic the trace phases include rutile, crichtonite, and glass (due to contamination with Si from the SiC rod). The murataite is represented by three different polytypes with five- (5C), eight- (8C), and three-fold (3C) fluorite unit cell composing a core, intermediate, and rim zone of the murataite grains, respectively (Fig. 3A, b). Diffraction peaks of murataite can be subdivided based on major reflections of 2.845, 2.833, and 2.805 Å corresponding to the 5C, 8C,

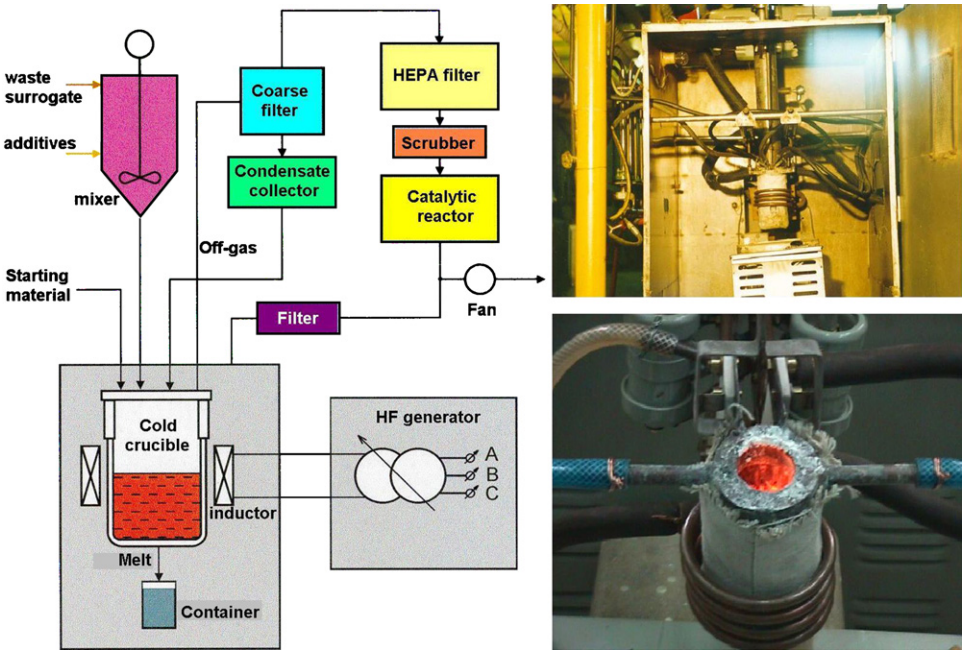

Fig. 1. Flowsheet of the Radon bench-scale ICCM unit (160 kW, 1.76 MHz) (left), installation of the bench-scale cold crucible in the process box (upper right) and view of lab-scale cold crucible unit (10 kW, 5.28 MHz) (lower right).

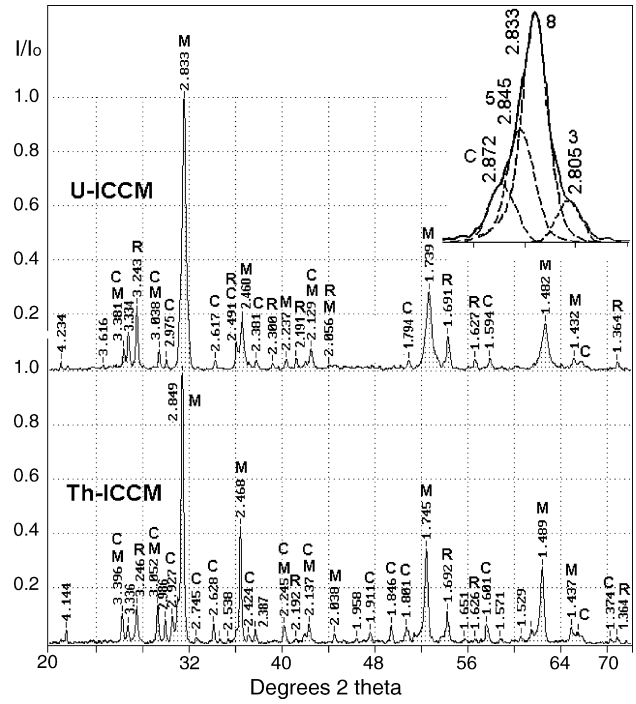

Fig. 2. XRD patterns of the U- and Th-bearing murataite-based ceramics and computer modeling of the major peak (inset). M: murataite polytypes, C: crichtonite, R: rutile; inset: 5, 8, 3—5C, 8C, and 3C polytypes, respectively; solid line: experimental, dotted lines: simulation.

and 3C polytypes, respectively.The formulae of the three murataite polytypes were calculated based on the qualitative EDS data (Table 1) and indicates the following compositions: $Ca_{2.54}Mn_{1.54}U_{0.56}Zr_{0.88}Ti_{7.80}Fe_{0.81}Al_{0.87}O_{27-x}$ (5C), $Ca_{4.33}Mn_{3.00}U_{0.86}Zr_{1.10}Ti_{13.51}Fe_{1.42}Al_{1.78}O_{47-x}$ (8C), and

Table 1
Chemical composition (wt%) of co-existing phases in the U-ICCM sample

Oxides	M5	M8	M3	Rutile	Crichtonite	Glass
Na_2O	–	–	–	–	–	3.31
Al_2O_3	3.57	4.33	9.19	–	6.73	18.34
SiO_2	–	–	–	–	0.50	31.26
K_2O	–	–	–	–	–	0.72
CaO	11.45	11.52	9.23	–	4.52	17.83
TiO_2	50.14	51.23	52.46	93.36	65.65	13.46
MnO	8.78	10.06	11.74	–	9.93	11.24
Fe_2O_3	5.21	5.37	9.14	0.82	9.67	2.45
ZrO_2	8.71	6.46	2.98	4.59	0.71	–
UO_2	12.14	11.03	5.24	1.23	2.23	1.39
Total	100.00	100.00	100.00	100.00	100.00	100.00

$Ca_{1.37}Mn_{1.37}U_{0.16}Zr_{0.20}Ti_{5.45}Fe_{0.95}Al_{1.50}O_{20-x}$ (3C). Based on crystal chemistry constraints and assuming a balance of 60–70% Mn^{2+} to 40–30% Mn^{3+} [16], the adjusted formulae would then be: $(Ca_{2.54}U_{0.56}Zr_{0.88}Mn^{2+}_{1.02})(Mn^{3+}_{0.52}Fe^{3+}_{0.81}Ti_{0.67})(Ti_{7.13}Al_{0.87})O_{25.34}$ (5C), $(Ca_{4.33}U_{0.86}Zr_{1.10}Mn^{2+}_{0.71})(Mn^{2+}_{1.29}Mn^{3+}_{1.00}Fe^{3+}_{1.42}Ti_{0.29})(Ti_{13.22}Al_{0.78})O_{42.07}$ (8C), and $(Ca_{1.37}U_{0.16}Zr_{0.20}Mn^{2+}_{1.27})(Mn^{3+}_{0.10}Fe_{0.95}Ti_{0.95})(Ti_{4.50}Al_{1.50})O_{18.09}$ (3C). Maximum UO_2 content (12.1%) was recorded in the core zone (5C polytype) and the average concentration of UO_2 in the rim zone is much lower (5.2%)—see Table 1. The mineral formulae of rutile and crichtonite were calculated as $Ti_{0.96}Zr_{0.03}Fe_{0.01}O_{1.99}$ and $Ca_{1.45}U_{0.15}Zr_{0.13}Mn_{2.30}Ti_{13.95}Fe_{1.85}Al_{2.02}O_{38.00}$, respectively. As can be seen from Table 1 the majority of the UO_2 is contained in the murataite; the UO_2 contents in crichtonite and glass are negligible. In short, the chemical compositions of the various phases, listed in Table 1, show that murataite polytypes are

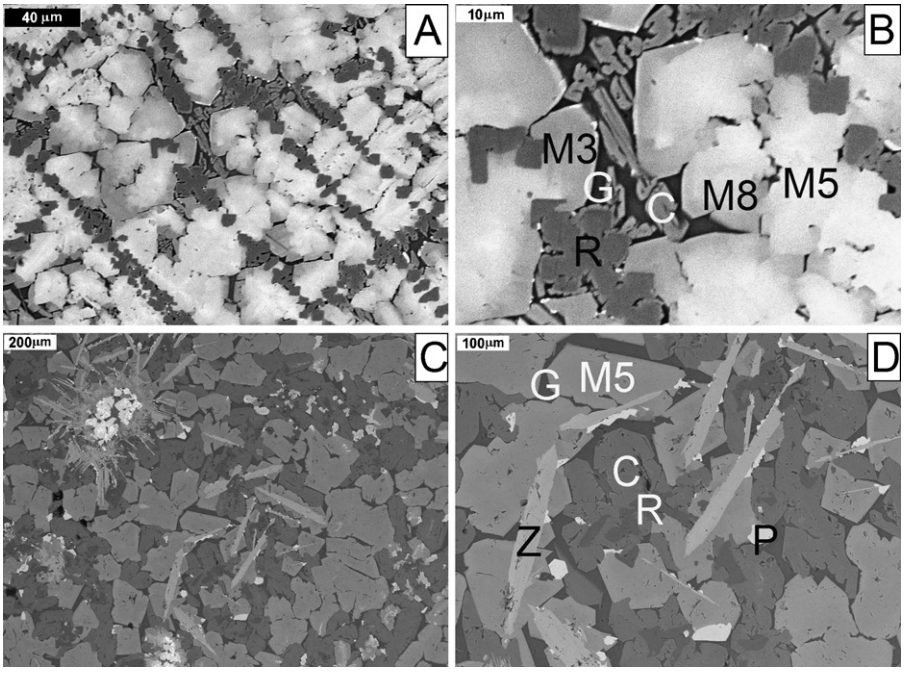

Fig. 3. SEM-images of the ceramics U-ICCM (A, B), Th-ICCM (C, D). C: crichtonite, G: glass, M3, M5, M8: murataite polytypes 3C, 5C, and 8C, respectively, P: pyrochlore, R: rutile, Z: low-symmetry phase (possibly zirconolite or thorutite); (B) and (D) are details of (A) and (C), respectively. Aggregates of undissolved thorianite grains are seen on picture (C).

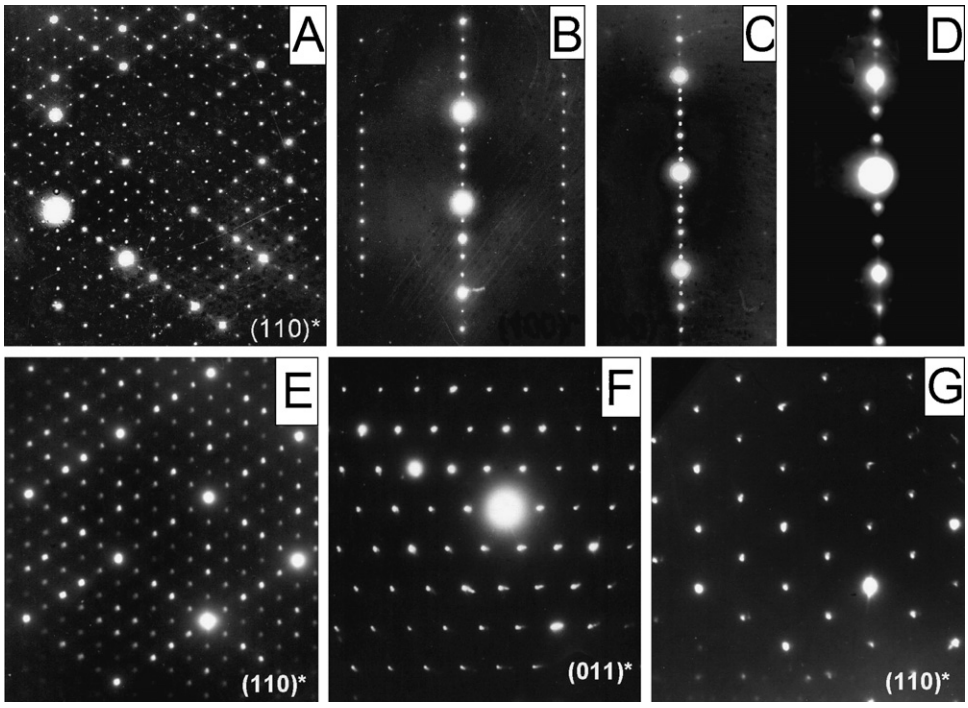

Fig. 4. SAED patterns of the murataite polytypes 5C (A, B, E), 8C (C), 3C (D), crichtonite (F), and pyrochlore (G) in the U-ICCM (A–D) and Th-ICCM (E and F) ceramics.

the major host phases for uranium and zirconium, as well as potential corrosion products (iron group elements—Fe, Mn).

3.2. Preparation and characterization of the Th-bearing ceramic

The Th-ICCM ceramic was produced in the lab-scale crucible in amount of approximately 1 kg. It is composed of major murataite (5C polytype) and crichtonite, minor thorianite, pyrochlore, and low-symmetry phase (Figs. 2, 3C, D and 4E, F).

In contrast to the U-ICCM ceramic, the Th-ICCM ceramic contains only the 5C polytype with the proposed formulae of $(Ca_{2.13}Mn_{1.90}Zr_{0.82}Th_{0.55}Fe_{0.78}Ti_{7.86}Al_{0.96}O_{27-x})$. Considering multiple manganese oxidation states, a ratio of Mn^{2+} to Mn^{3+} was used to satisfy site occupancy constraints. The proposed formulae is then $(Ca_{2.13}Th_{0.55}Zr_{0.82}Mn^{2+}{}_{1.50})(Mn^{3+}{}_{0.40}Fe^{3+}{}_{0.78}Ti_{0.82})(Ti_{7.04}Al_{0.96})O_{25.30}$. As discussed previously, the distribution of Th in murataite is uniform. The chemical composition of crichtonite/loveringite (Table 1) is recalculated on a 38-oxygen basis: $Ca_{1.62}Mn_{2.52}Th_{0.30}Zr_{0.47}Ti_{13.27}Fe_{1.76}Al_{1.84}Si_{0.19}O_{38.00}$. Pyrochlore is present as light-colored inclusions (detected by backscattered electron imaging) whose average chemical composition (Table 2) corresponds to $Ca_{0.64}Mn_{0.39}Fe_{0.05}Zr_{0.15}Th_{0.65}Ti_{2.12}O_{6.92}$. The occurrence of aggregates of partly altered thorianite (ThO_2) crystals and rutile due to incomplete dissolution of Th dioxide from its precursor was noted. In addition, the presence of rare, elongated crystals characterized by low symmetry crystal lattice (probably monoclinic) that we tentatively identify as zirconolite were detected. The proposed formulae of this phase is $(Ca_{0.57}Mn_{0.34}Th_{0.09})(Zr_{0.47}Th_{0.18}Ti_{0.35})(Ti_{1.74}Fe_{0.14}Al_{0.12})O_7$. An apparent deficiency of Zr^{4+} in the Zr-site may be mitigated by the incorporation of Th^{4+} and Ti^{4+}, which, although possessing different ionic radii, may stabilize the zirconolite structure. This phase, as well as thorianite and rutile, are presumably a product of incomplete reactions.

Table 2
Chemical composition (wt%) of co-existing phases in the Th-ICCM sample

Oxides	M5	Crichtonite	Low-symmetry phase	Pyrochlore	Rutile	Thorianite	Glass
Al_2O_3	3.96	5.47	1.78	0.33	0.43	–	15.60
SiO_2	–	0.67	–	–	–	–	34.69
CaO	9.63	5.32	8.55	8.42	–	–	21.96
TiO_2	50.49	61.87	44.94	39.41	93.77	1.47	10.11
MnO	10.88	10.44	6.44	6.47	0.00	–	14.01
Fe_2O_3	5.05	8.21	3.36	0.94	0.43	–	2.43
ZrO_2	8.18	3.39	15.51	4.42	5.37	–	–
ThO_2	11.81	4.63	19.42	40.00	0.00	98.53	1.21
Total	100.00	100.00	100.00	100.00	100.00	100.00	100.00

4. Discussion

The pyrochlore structure has two cationic positions: "A" filled with large-sized cations $An^{3+/4+}$, $Ln^{3+/4+}$, Ca^{2+}, Mn^{2+}, Na^{+}, and "B" occupied by smaller cations Ti^{4+}, Zr^{4+}, Hf^{4+}, Sn^{4+}, Nb^{5+}, Ta^{5+}, Mo^{4+}. The murataite structure has four cationic sites: "A", "B", five-coordinated "C" filled with $Mn^{2+/3+}$ and $Fe^{2+/3+}$ ions, and tetrahedral "T"-sites which are normally empty in the synthetic murataites. Alternating of the pyrochlore and murataite modules in the structure of the polytypes creates conditions for accommodating most of the elements occurring in complex REE/actinide-bearing wastes.

Although there are a number of methods to produce murataite/pyrochlore ceramics, we suggest that the melting route provides a superior method for crystal growth during melt crystallization. This method yields zoned crystals of the pyrochlore/murataite series with the highest concentrations of actinides and rare earth element isolated in the core of the host crystals. At the first step at the highest temperature, nucleation centers of the phase with the highest melting point are segregated. In the given system this is the phase enriched with actinide and/or rare earth elements. In principle, this could be the pyrochlore as it appears in the systems with heavy rare earths $HREE_2O_3$–MnO_x–TiO_2 [17,18]. Thus the residual melt is depleted with HREEs and the secondary segregated phase is 7C or/and 5C with lower HREE and higher Mn contents. However, in our case, the actinide concentration (10 wt%) is rather low and the first nucleating phase is the 5C composing core of the grain. Crystals of the 8C phase with lower actinide and zirconium content are overgrown on the nuclei of the 5C phase forming zoned structure of the grain. The rim is composed of the 3C phase with the lowest actinide and zirconium content. The 3C phase (nominal murataite) has low isomorphic capacity with respect to the actinides (and light rare earth—LREE-Ce-group) – its natural analogue is a mineral of HREEs – Y-group. As a result, residual actinides/rare earths enter crichtonite.

The ICCM is very high-productive process for actinide waste forms fabrication. Application of a larger-scale (108 mm in diameter) cold crucible provides for low-melt cooling rate in both crucible and filled container with sequential crystallization of various murataite polytypes. Crystal growth under these conditions yields dense ceramics with zoned structure of the grains with maximum actinide concentration in the core and minimum in the rim thus reducing their leachability.

Finally, we note that the set of run products appears to be dependent upon the size of the crucible in which melting and crystallization occurs. Melt cooling rates in small cold crucibles are faster and rapid crystallization resulted in formation of only the 5C murataite polytype characterized by a uniform distribution of elements in its matrix. Thus, application of large-scale cold crucibles is a prospective route for the development of industrial-scaled process and technology for ceramization of actinide-bearing HLW. The advantage of this method is that it produces zoned crystals with the highest concentrations of actinides and rare earth elements in the core, effectively isolating these elements from potential leach solutions.

5. Conclusion

Murataite-based ceramics doped with 10 wt% of either UO_2 or ThO_2 were produced by the ICCM in 108 and 65 mm inner diameter cold crucibles. Larger sized cold crucible provides for conditions for crystallization of zoned grains composed of murataite polytypes 5C → 8C → 3C with consequently reduced actinide content from core to rim of the grains creating multi-barrier protection against leachate attack. Higher cooling rates taking place in small crucibles yield the only murataite polytype (5C) while the rest of the actinides enter extra phases.

Acknowledgements

The research was supported by Office of Basic Sciences of the US DOE (Project RUC2-20009-MO-04). Authors thank Ms. Maria Zen'kovskaya for her participation in ICCM runs.

References

[1] Yu.S. Kuz'minov, E.E. Lomonova, V.V. Osiko, High-Fusible Materials from Cold Crucible, Nauka, Moscow, 2004 (Russian).
[2] R. Do Quang, V. Petitjean, F. Hollebecque, et al., Proceedings of the Waste Management '03 Conference, Tucson, AZ, 2003, CD-ROM.
[3] A.P. Kobelev, S.V. Stefanovsky, O.A. Knyazev, et al., Proceedings of the 107th Annual Meeting of the American Ceramic Society, Baltimore, MD, 10–13 April, 2005, CD-ROM.
[4] I.A. Sobolev, S.A. Dmitriev, F.A. Lifanov, et al., Glass Technol. 46 (1) (2005) 28–35.
[5] V.I. Vlasov, O.L. Kedrovsky, A.S. Nikiforov, et al., Back End of the Nuclear Fuel Cycle: Strategies and Options, IAEA, Vienna, 1987, pp. 109–117.
[6] I.A. Sobolev, S.V. Stefanovsky, S.V. Ioudintsev, et al., Mater. Res. Soc. Symp. Proc. 465 (1997) 363–370.
[7] R.A. Day, J. Ferenczy, E. Drabarek, et al., Proceedings of the Waste Management '03 Conference, Tucson, AZ, 2003, CD-ROM.
[8] S.V. Stefanovsky, O.I. Kirjanova, S.V. Yudintsev, O.A. Knyazev, Proceedings of the Waste Management '01 Conference, Tucson, AZ, 2001, CD-ROM.
[9] P.E.D. Morgan, F.J. Ryerson, J. Mater. Sci. Lett. 1 (1982) 351–352.
[10] T.S. Ercit, F.C. Hawthorne, Can. Mineral 33 (1995) 1223–1229.
[11] V.S. Urusov, N.I. Organova, O.V. Karimova, et al., Trans. (Doklady) Russ. Acad. Sci./Earth Sci. Sec. 401 (2005) 319–325.
[12] S.V. Stefanovsky, S.V. Yudintsev, R. Gieré, G.R. Lumpkin, in: R. Gieré, P. Stille (Eds.), Energy, Waste, and the Environment: A Geological Prospective, Geological Society, London, 2004, pp. 37–63.
[13] R.C. Ewing, W.J. Weber, J. Lian, J. Appl. Phys. 95 (2004) 5949–5971.
[14] S.V. Stefanovsky, S.V. Yudintsev, B.S. Nikonov, et al., Mater. Res. Soc. Symp. Proc. 893 (2006) 429–434.
[15] J. Lian, L.M. Wang, R.C. Ewing, et al., Mater. Res. Soc. Symp. Proc. 807 (2003) 225–230.
[16] S.V. Stefanovsky, S.V. Yudintsev, B.S. Nikonov, A.A. Shiryaev, Proceedings of the Vth Conference on Radiochemistry-2006, Dubna, Russia, 23–28 October, 2006, pp. 212–213 (abstracts).
[17] O.I. Kirjanova, S.V. Stefanovsky, S.V. Yudintsev, Mater. Res. Soc. Symp. Proc. 757 (2003) 259–264.
[18] S.V. Stefanovsky, S.V. Yudintsev, B.S. Nikonov, O.I. Stefanovsky, Mater. Res. Soc. Symp. Proc. 932 (2006) 559–566.